Research Square

Preprints are preliminary reports that have not undergone peer review.
They should not be considered conclusive, used to inform clinical practice,
or referenced by the media as validated information.

Crystallinity determination for cellulose nanomaterials using powder X-ray diffraction coupled with Rietveld analysis: An interlaboratory comparison

Nayomi Plaza
Forest Products Laboratory
Alfred French
Forest Products Laboratory
C Driemeier
Brazilian Center for Research in Energy and Materials
B Duchemin
CNRS-Université le Havre Normandie
M Godinho
Universidade NOVA de Lisboa
C Honorato-Rios
University of Cambridge
K Ito
Rigaku Corporation
Jacobs Jordan
United States Department of Agriculture
S Kim
Materials Research Institute
O Kuznetsov
Scientific Metrology and Technology Directory
J Lee
Materials Research Institute
J Meija
National Research Council
J Pinto
Universidade NOVA de Lisboa
S Verpaele
BeCOH VZW
S Vignolini
University of Cambridge

N Wonderling
Materials Research Institute
Linda Johnson
National Research Council
Wadood Y. Hamad
wadood@seprify.com

Seprify AG

Research Article

Keywords: Cellulose nanocrystals, Cellulose nanofibers, Crystallite size, XRD, Statistical comparison

Posted Date: November 25th, 2026

DOI: https://doi.org/10.21203/rs.3.rs-9136443/v1

License: This work is licensed under a Creative Commons Attribution 4.0 International License.
Read Full License

Additional Declarations: No competing interests reported.

Crystallinity determination for cellulose nanomaterials using powder X-ray diffraction coupled with Rietveld analysis: An interlaboratory comparison

N. Plaza[1*], A. D. French[2*], C. Driemeier[3], B. Duchemin[4], M. H. Godinho[5], C. Honorato-Rios[6], K. Ito[7], Jacobs H. Jordan[8], S. H. Kim[9], O. Kuznetsov[10], J. Lee[9], J. Meija[11], J. V. Pinto[5], S. Verpaele[12], S. Vignolini[6], N. M. Wonderling[9], L. J. Johnston[11], W. Y. Hamad[13, 14]*

[1] N. Plaza, Forest Products Laboratory, Madison, WI 53726 USA

[2] A. D. French, US Department of Agriculture (retired), University of Vienna, Austria

[3] C. Driemeier, Brazilian Biorenewables National Laboratory (LNBR), Brazilian Center for Research in Energy and Materials (CNPEM), 13083-970, Campinas, SP, Brazil

[4] B. Duchemin, Laboratoire Ondes et Milieux Complexes, UMR 6294, CNRS-Université le Havre Normandie, 53 rue Prony BP540, 76058 Le Havre, France

[5] M. H. Godinho and J. V. Pinto, Departamento Ciência dos Materiais, Universidade NOVA de Lisboa, *Campus* de Caparica, 2829-516 Caparica, Portugal

[6] C. Honorato-Rios and Silvia Vignolini, University of Cambridge, Yusuf Hamied Department of Chemistry, Lensfield Road, Cambridge CB2 1EW, UK

[7] K. Ito, X-ray Research Laboratory, Rigaku Corporation, 3-9-12, Matsubara-cho, Akishima-shi, Tokyo, Japan

[8] J. H. Jordan, US Department of Agriculture, 1100 Allen Tousaint Blvd., New Orleans, Louisana, 70124 USA

[9] S. H. Kim, J. Lee, and N. M. Wonderling, Department of Chemical Engineering, Materials Research Institute, University Park, PA 16802, USA

[10] O. Kuznetsov, Scientific Metrology and Technology Directory, Materials Metrology Division, INMETRO, Brazil

[11] J. Meija and L. J. Johnston, Metrology Research Centre, National Research Council, Ottawa, Canada K1A 0R6

[12] S. Verpaele, BeCOH VZW, Technologiepark 122, 9052 Zwijnaarde, Belgium

[13] W. Y. Hamad, Transformation and Interfaces Group, Bioproducts Innovation Centre of Excellence, FPInnovations, 2665 East Mall, Vancouver, BC, Canada V6T 1Z4

[14] Current address: Seprify AG, Route de l'Ancienne Papeterie 180, 1723 Marly, Switzerland

*Corresponding authors: wadood@seprify.com, adfrench@cox.net, nayomi.plazarodriguez@usda.gov

Abstract

Cellulose nanomaterials are slowly gaining ground in the manufacturing realm. As part of ongoing efforts to provide quality assurance measures for reproducible production of cellulose nanomaterials, powder X-ray diffraction (PXRD) can be an accessible and relatively easy technique to use to establish percent crystallinity measurements as a quality control and assurance standard of these materials. An interlaboratory comparison (ILC) was undertaken to test a protocol for data acquisition and determination of percentage crystallinity and crystallite size for cellulose nanomaterials using PXRD coupled with peak fitting of the diffraction pattern by Rietveld analysis. Parameters such as the exact unit cell dimensions and crystallite size were adjusted by the software to minimize the difference between the calculated and observed patterns by the least-squares method. The significant differences in these values for the nanocellulose samples derived from wood pulp compared to the parameters from the tunicate structure that provides our ideal pattern arise in part because of biosynthetic mechanisms that result in the crystallites of different sizes and shapes. This paper outlines the methodological approach along with comparison of the results and site-dependent variability. Conclusions are made as to the most practical and technically consistent steps for quantifying the crystallinity of nanocellulose.

Keywords

Cellulose nanocrystals; Cellulose nanofibers; Crystallite size; XRD; Statistical comparison

Introduction

Cellulose nanomaterials (CNMs) are a family of emerging bio-based products with significant potential commercial impact. Their production from abundant cellulose sources such as wood pulps or agricultural and food-processing waste makes them candidates for use as non-toxic, biodegradable and sustainable nanomaterials for a wide range of applications, including those that currently use petroleum-based components. Several types of cellulose nanomaterials are currently produced on pilot, pre-commercial or commercial scales (Global Market 2024). Realizing the full potential of these materials requires standard methods for characterization of a range of material properties (Foster et al. 2018), including crystallinity. Crystallinity is an indication of material quality, success of processing and degradation of the material during processing. Collectively, these aspects can affect the extent of surface modification, for instance, and the performance for various applications in multi-component systems, such as polymer composites and colloidal suspensions. Crystallinity is also important for distinguishing between CNM grades and products, as well as ensuring batch control and repeatability. It may further provide information on the cellulose source and production method.

Crystallinity of cellulose nanomaterials is defined as the fractional crystalline contribution relative to the total crystalline and amorphous contributions in the material. There are several approaches for measuring crystallinity of materials, including powder X-ray diffraction (PXRD), differential scanning calorimetry or solid-state nuclear magnetic resonance (Park et al. 2010; Daicho et al. 2018; Salem et al. 2023). Each of these techniques has its merits and limitations. The use of crystallinity for quality control of CNM production and further processing requires a method that can quickly, routinely, and reproducibly be implemented and one that is easily accessible and can be run in most laboratories with the same level of proficiency. PXRD has the potential to address these criteria (see Fig. 1).

Among the above methods, signals from diffraction methods are created based on the general periodic arrangement of the atoms and thus might be the most direct approach. Other methods are often based on certain signals that have been correlated with results from diffraction studies. In NMR, the crystallinity estimation is based on signals from the C4 atom that are influenced by the orientation of the C6 primary alcohol group. The molecules of the native cellulose allomorphs Iα and Iβ, especially those on the interior of the crystallites, have the C6 hydroxyl group in the tg orientation.[1] On the other hand, those groups in the mercerized or regenerated cellulose II allomorphs, as well as a majority of the amorphous forms take the gt form. Thus, the changes in the balance between the chemical shift of the C4 atom at 89 ppm for crystalline cellulose I to chemical shifts at 84 ppm, the often-used

[1] Having an O5-C5-C6-O6 torsion angle of about 180° (trans) and a C4-C5-C6-O6 torsion angle of roughly -60° (gauche).

indicator of amorphous fraction, are primarily due to these changes in O6 orientation (Yang et al. 2018; Yang and Kubicki 2020). From this it is clear that the popular NMR method is not as direct as diffraction, but also that different results may be expected from the two methods. Indications of crystallite size from NMR might consider that the surface molecules are not part of the crystal, whereas the deviations from the tg orientation of surface molecules would have less effect on the diffraction pattern. This is especially so because the O6 x- and y-coordinates for tg and gt are somewhat similar. Only the x- and y-coordinates affect the strong cellulose 1 -1 0, 1 1 0, and 2 0 0 peaks.

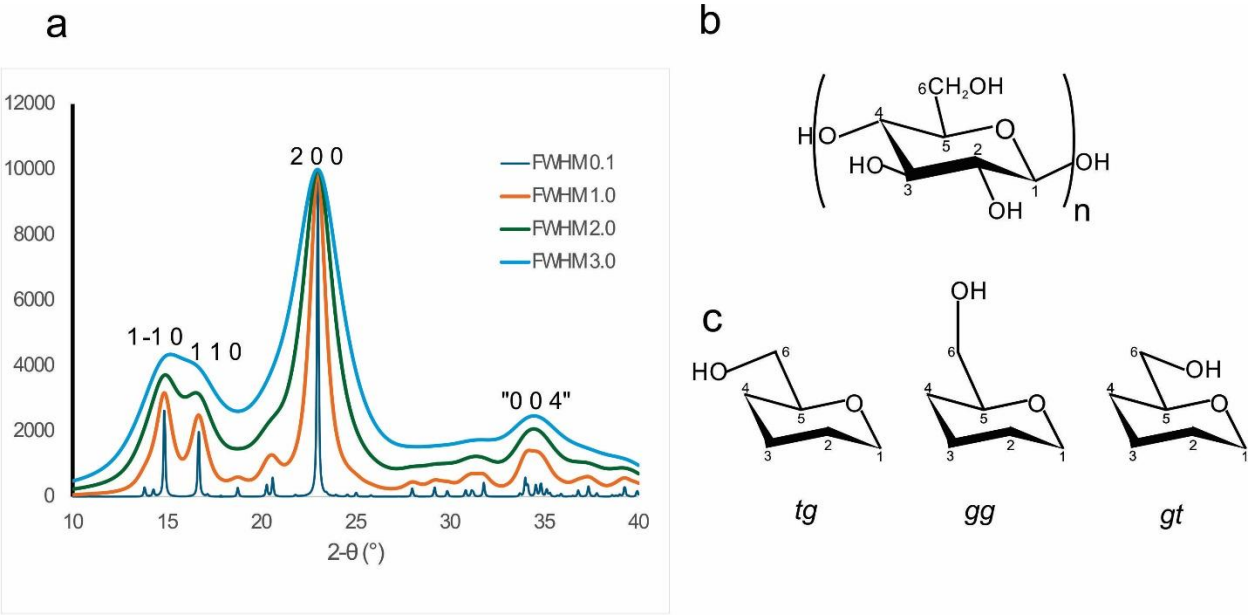


Fig. 1 a) Calculated diffraction patterns with peak widths Full Width at Half Maximum (FWHM) (or peak width at half maximum, pwhm) corresponding to crystallite sizes of 90.0 nm, 9.0 nm, 6.0 nm, 4.5 nm, and 3 nm (K in the Scherrer equation =1) for FWHM values of 0.1, 1.0, 2.0, and 3.0 with Mercury (Macrae et al. 2020) and the Nishiyama et al. (2002) crystal information file. These calculated patterns have no background, no amorphous content, no preferred orientation, and the crystallites have isotropic sizes. The Miller indices of the most important peaks are shown, with the "0 0 4" peak in quotation marks because the 0 0 4 peak is one of the smaller peaks in the cluster when there is random orientation of the crystallites. b) A glucose residue as the repeating unit of cellulose with numbering of the carbon atoms. c) A depiction of the three staggered conformers of the C_6OH group.

For routine studies of nanocellulose crystallinity with diffraction, the powder diffraction method is the most practical. Although fiber diffraction has the possibility to present far more detailed information because the data are much less-overlapped, it would be impractical to create fiber-type samples from the nanocellulose materials that comprise the samples herein. An example of such a laborious preparation is from Nishiyama et al. (1997).

Still, it would be of great interest to confirm the findings of PXRD studies with results taken from fibers of related materials. Samples similar to those from the present study that form fibers when subjected to otherwise comparable treatments should receive a comparable study by fiber diffraction to validate the type of work herein on powdered samples. To date, fiber methods have been directed towards determination of the crystal structure, with less emphasis on the degree of crystallinity or the crystallite size.

Several sources of radiation having wavelengths suitable for these studies include electron microscopes and neutron beams. In short, however, neutrons are only available at relatively few sources in the world, and electron diffraction of cellulose is a high-skill talent because cellulose quickly burns up in the electron beam. In alignment with the above call for fiber diffraction analyses for confirmation of the PXRD methodology, it is noted that selected-area electron diffraction could potentially carry out analyses on even the nanometer sized cellulose crystallites for a complementary analysis.

Among the X-ray sources, the laboratory diffractometer is reasonably available. Technology continues to evolve, especially in the detectors used in these machines. Even in the benchtop versions, detectors are now used that simultaneously count photons from various extents of the entire 2θ range. Some of the most recent detectors can do photon energy discrimination so that not only the $K\beta$ radiation is avoided, but even $K\alpha 2$ is essentially suppressed. Alternatively, a much simpler system with a 2-D detector could be used. Samples could be packed into a capillary tube or even simply packed into a pinhole in a plastic sheet for transmission studies. Still, for high throughput, the modern powder diffractometer has the advantages of convenience and of potentially including autoloading of samples. The modern detectors can process a sample in a few minutes, and the expenditure of more than a half hour is a waste of diffractometer tube life for a straight-forward PXRD analysis.

Besides the loss of information inherent in powder diffraction, the methods of analyzing the data are not remotely uniform, or even carried out correctly within the guidelines of the proposed methods. For example, the widely used approach of Segal et al. (1959) for estimating crystallinity utilizes the height of the 2 0 0 peak and the minimum intensity between the 1 1 0 and 2 0 0 peaks as measures of the crystalline and amorphous content, respectively. See how the point at about 18.6° of amorphous intensity varies with crystallite size in Fig. 1 for perfectly crystalline patterns. Another popular method is known as the peak area or the peak deconvolution method, dating to Hermans and Weidinger (1948), that has been greatly facilitated by contemporary software. Instead of Segal's minimal technology approach (a ruler for two intensity measurements and elementary school arithmetic), the peak area method accounts for the observed pattern with, typically, three to five peaks to account for the observed peaks, plus an amorphous contribution from a broad "hump" to make up the difference. The variables include the peak locations, heights, and their widths

at half height. Again, see Fig. 1 for the numerous small peaks that contribute to the pattern despite not being individually visible in patterns from the realistic crystallite sizes. Other approaches have also been explored. Summaries and comparisons of these methods are available (Thygesen et al. 2005; Hamad and Hu 2010; Park et al. 2010; French 2020; Salem et al. 2023).

Here we describe an interlaboratory comparison (ILC) that was undertaken to test a protocol for data acquisition and determination of percentage crystallinity and crystallite size for cellulose nanomaterials using PXRD coupled with peak fitting of the diffraction pattern by Rietveld analysis. In our usage for cellulose samples, the Rietveld (1960) method matches an experimental diffraction profile with a modelled pattern based on known atomic coordinates for the crystal structure of a cellulose allomorph. Parameters for the known structure, such as the exact unit cell dimensions and crystallite size, are adjusted by the software to minimize the difference between the calculated and observed patterns by the least-squares method. The significant differences in these values for the nanocellulose samples derived from wood pulp compared to the parameters from the tunicate structure that provides the reference pattern for this study arise in part because of biosynthetic mechanisms that result in the crystallites of different sizes and shapes.

The Rietveld method was initially developed to handle the crystal structure determination (x-, y-, and z-coordinates of the individual atoms) for samples that could not provide single crystals of a suitable size for neutron diffraction. The basic problem of PXRD is that all diffraction spots with similar 2θ values will make overlapping rings of intensity. To get the individual h k l values used in a single-crystal study, some sort of peak deconvolution would be needed, a task more prone to error.

The Rietveld method simply models the whole diffraction pattern by calculating the intensity at each 2θ point in the pattern. To do this, it was necessary to include the influence of the factors that distort observed powder data from those expected from an ideal or prototype crystal. In any structural study of cellulose, there will be minor variations in the unit cell dimensions. The presence of another phase, or some amorphous scattering, are likely. Problems not inherent in single crystal work include the samples having crystallite size anisotropy, *i.e.*, the crystallites have different dimensions along the a-, b-, and c-axes. Further, in part because of size anisotropy and different surface potentials, the particles of nanocellulose will not necessarily fall into the sample holder with the random orientation needed so that all crystal planes have an equal chance of being in the Bragg position. The condition where one group of planes is more likely to lie parallel to the sample holder is called “preferred orientation” and it, as well as crystallite strain and size anisotropy are aspects of “texture”. All cellulose samples are prone to disruptive aspects of texture. Sample particles of microcrystalline plant cellulose as well as cut up fibers retain the tertiary structure of the fiber that tends to be longer than its cross-section size and will therefore tend to lie in the plane of a sample holder used for reflection-mode PXRD. This will favor the equatorial (h k 0) reflections and dis-favor the meridional (0 0 ℓ) reflections. However, the preserved aspects of

a cell wall in such particles preserves a rotational diversity about the fiber axis for the individual crystallites, avoiding favoring the (h k 0) reflections. This restraint is lost for nanocellulose that has been freed from the cell wall structure. Bacterial cellulose is excreted as individual nanofibrils that, depending on conditions as synthetic medium and degree of agitation, are prone to association in pellicles, have substantial preferred orientation with the (1 0 0) planes of the triclinic Iα unit cell in the plane of the sample holder. This produces a pattern with a dramatic increase in the 1 0 0 peak intensity, relative to the 0 1 0 peak that can be nearly absent and the 1 1 0 peak, dominant for random patterns, be reduce to a height lower than for the 1 0 0 peak of pellicle samples.

The nanocellulose samples used for this ILC have the potential for preferred orientation, particularly owing to aggregation from the drying technique used to prepare the sample. As nanocellulose is often delivered as a suspension or slurry, the sample drying may be pre-formed as part of the diffraction analysis; the presence of substantial water will affect the diffraction pattern (Fang and Catchmark 2014) and complicate the crystallinity analysis.

One of the issues in any determination for a given batch of material is obtaining a representative sample. This is a more demanding task for crystallinity of nanocellulose materials. In some cases, the extent of preferred orientation in a sample is an important characteristic, potentially as important as the degree of crystallinity or the crystallite size. In the case of samples delivered as slurries or never-dried suspensions, it is important to dry the samples in such a way that as much preferred orientation be avoided as possible. This could reduce negative impact of the powerful algorithms in Rietveld software that compensate for the inevitable preferred orientation of cellulosic samples.

The task of this ILC project is to do the analyses based on a set of three samples that are as randomly oriented as possible to be representative of the sample. The instrument configuration and detector sensitivity are also important as the presence of noise in the pattern results in less guidance from the data. The noise, or point-to-point random variation in the observed intensity, is proportional to the square root of the intensity. Thus, to reduce the noise by half, it is necessary to increase the counting time at each 2θ point by a multiple of four. If the data are noisy, it may be that a sophisticated smoothing algorithm, such as Savitzsky-Golay, would be useful but simple moving average smoothing is not a likely improvement. The ILC was undertaken to provide the pre-normative data required to support the development of a technical specification at ISO Technical Committee 229 – Nanotechnologies (ISO TS 23361, 2024).

Experimental

Samples

Three CNM samples derived from wood pulp were used in the ILC: (1) a CNC reference material released by the National Research Council Canada and produced by sulfuric acid hydrolysis of softwood pulp followed by neutralization, sodium exchange, purification and freeze-drying.

Sulfuric acid hydrolysis generates sulfate half-ester groups on the surfaces, and a detailed characterization of this material is summarized in (Jakubek et al. 2018); (2) a CNF sample purchased from University of Maine and obtained from wood pulp as a freeze-dried powder; and (3) an iCNF sample kindly provided by Oji Holdings Corporation, Japan and produced from wood pulp by TEMPO-oxidation followed by freeze-drying. The CNF and iCNF samples were milled using a laboratory Wiley Mill with a 0.5 mm sieve opening to ensure uniform particle size prior to preparing samples to send to ILC participants.

ILC Design and Participating Laboratories

The ILC was conducted under VAMAS Technical Working Area 34 (nanoparticle populations) and was organized in three phases. Phase 1 recruited participants and obtained their input on the initial protocol which was based on experiments carried out at FPInnovations in Vancouver, BC, Canada. Phase 2 tested the protocol for Rietveld analysis using a data set consisting of diffraction data for the three CNM samples. The initial protocol was modified based on the input of the participants and the results obtained in the tests of the Rietveld analysis protocol. In Phase 3 participants were sent the three samples and requested to measure three replicates per sample, to analyze the data using the Rietveld method and to return the raw data, modeling results, instrument parameters and modeling software and options used.

Ten participating institutions from Asia, Europe and North and South America completed Phase 3 of the ILC and one other laboratory participated in Phases 1 and 2 of the ILC. The 10 laboratories that completed Phase 3 included four universities, one industrial, and five government laboratories.

Data acquisition protocol

Sample preparation was carried out by packing the dry powdered CNM into the sample holder, preferably a zero background cell to minimize background signals, and levelling the surface that would be exposed to the X-ray beam with a blade. This is the normal sample preparation method for data collection in Bragg-Brentano[2] configuration for Rietveld modelling. The protocol is appropriate for powder X-ray diffractometers in the Bragg-Brentano configuration and equipped with a copper X-ray tube and a position sensitive detector. Other X-ray sources are acceptable provided that the resolution and angular range are similar. The instrument configuration should be capable of removing CuKβ radiation from the measurement, for example using a Ni-filter and rotating the sample holder for data collection. It was recommended to set up the instrument according to the manufacturer's recommended procedure and to measure a standard (*e.g.*, alumina)

[2] The Bragg-Brentano geometry has two modes of data collection. In one of these reflection modes, the divergent beam comes from an X-ray tube that is stationary, the sample holder is moved by θ, and converging diffracted beam is the detector is moved by 2θ. The other mode has both the tube and the detector moving simultaneously, each at θ while the sample stays horizontal. Horizontal sample holders have numerous advantages, including averaging some preferred orientation by spinning the sample in the horizontal plane, not needing adhesive to retain the sample, and provision for heating or pressure systems.

to ensure proper calibration. Examples of suitable fixed slit configurations were provided for 3 different diffractometers for reference purposes.

Scattering data was to be collected from an angular range of 5° to 90° in 2θ (or 5° to 60° if necessary to minimize data collection time), with a step size (sampling interval) of $\Delta 2\theta = 0.04°$. The counting time per step was selected so as to collect a minimum of 30,000 counts at the position of maximum intensity in the area corresponding to d-spacings of 6 to 3.5 Å (15° to 25° 2θ with 1.5418 Å CuKα radiation). An environmental background scan was collected using the same conditions but an empty sample holder to identify possible background signals related to the sample holder or choice of slits. Three replicate measurements on different aliquots were requested for each sample. Scattering from a standard crystalline sample (e.g., quartz) was measured, depending on the available method used to determine the contribution of instrumental factors to line broadening

Rietveld analysis protocol

Software that is capable of Rietveld analysis is optional with diffractometers from Bruker, Malvern and Rigaku. Either the native diffractometer software or a free software package such as MAUD, a Java based package for material diffraction, are recommended. An important software requirement is that the X-ray powder line profile fitting must take into account the contribution of the instrument configuration to the peak shape and width for the diffraction pattern. This may be accomplished using the fundamental parameters approach which is available in some software packages and uses physically based models to generate the line profile shapes (Cheary et al. 2004, Mendenhall et al, 2015). Alternately, the user can measure a standard crystalline sample with the same instrument geometry to be used for the cellulose samples and fit the diffraction pattern to the Cagliotti equation to obtain the instrument response. Participants were provided with the crystallographic information file (CIF) for cellulose 1β, the typical structure for wood pulp derived CNM, from the Crystallography Open Database (http://www.crystallography.net). The CIF (#4114995) is based on neutron data for tunicate-derived cellulose obtained by Nishiyama et al. (2002). Note that CIF 4114994 does not contain the hydroxy hydrogen atoms.

The diffraction data and CIF files were read in, and the scale factor and crystal size/peak width were adjusted in order to compare the observed pattern and the one calculated from the CIF. Because the broad peaks of cellulose are so different from the default sharp peaks assumed in the software, these two variables should be reasonably close to providing a suitable pattern before any refinement is begun.

It was recommended to subtract the environmental background (if necessary) prior to Rietveld analysis. The environmental background, consisting primarily of air scatter, is best recorded as a blank run on the smooth side of a "zero-background" sample holder. Some software has a provision for loading such a blank run specifically as background data. Even so, it may still be useful to refine an additional background as a second order polynomial. Two options are recommended for

the amorphous component since there was a lack of consensus among participants as to the optimal approach: (1) A broad peak defined by a polynomial function (*e.g.*, a Chebyshev polynomial with coefficients 0,1) and based on the fundamental parameters geometry and a minimum crystal size (for instance, 0.3 nm) to ensure an amorphous peak shape rather than a shape that looks like the modelling background, or (2) a cellulose II crystallite with a 1.2 nm size. Although the 1.2 nm crystallite size gives a good approximation to a range of observed amorphous cellulose patterns, a following refinement of that 1.2 nm value may lead to a small amount of cellulose II with a suitable size to be considered as a crystalline material instead of an amorphous component. Several CNM preparation methods are known to produce varying amounts of cellulose II and they are difficult to observe in diffraction patterns when the amount is less than 20%. A fitting range 10° to 60° 2θ was specified for both options. The unit cell of the cellulose structures is then allowed to refine within reasonable parameters. The goodness of fit parameter should be tracked to determine whether the model improves. It is useful to keep a record of the order in which parameters are adjusted during refinement and the values for both residuals Rb and Rwp as well as goodness of fit at each step. There should be a minimum of four different stages of the refinement, with new additions of variables at each stage. Those with the most important visual affects could be added first. The crystallite size/peak shape is refined employing a double-Voigt approach, correcting for both Lorentzian and Gaussian contributions to crystallite size peak broadening. The proportion of Lorentzian and Gaussian contributions will depend on the software. As a starting point one can select 0.75 Lorentzian, 0.25 Gaussian. Other approximations for correction can be used as an alternative to the double-Voigt approach (*e.g.*, pseudo-Voigt), and will work well for most cases.

A preferred orientation correction is required for samples that have some alignment of particles. This can be accomplished with one of two options in most software packages. The March-Dollase correction (Dollase 1986) (1 parameter) is simpler and will be adequate in most cases. This approach is recommended for use with MAUD software. Alternatively, the spherical harmonics correction with order of 6 can be used and is recommended with TOPAS. A refinement cycle using one of the two corrections should be used to correct for possible orientation effects. Finally, a correction for anisotropic broadening (Popa and Balzar 2008) can be employed, if available in the software used. Some spray-dried packed CNC samples show a sharp feature at ~35° 2θ. This feature may be due to anisotropic broadening effects of the cellulose nanocrystals showing an elongation of the crystal along the molecular axis. A similar feature has been observed previously in diffraction patterns of cotton fibers obtained using synchrotron radiation; the feature is assigned to the (0 0 4) meridional peak (visible for the CNC patterns in Fig. 3a and in Supplementary Information Fig. S1) and its intensity varies with the degree of orientation (French and Kim 2018).

The percent crystallinity of the sample is calculated by dividing the crystalline area (A_{cry}) over the sum of the crystalline and amorphous (A_{amor}) areas, determined by the deconvolution approach (Hamad and Hu 2010).

$$\% \text{ crystallinity} = (A_{cry}/(A_{cry} + A_{amor})) \times 100 \qquad \text{Eq 1}$$

The MAUD software provides the percentage for each of the modelled phases (*e.g.*, crystalline and amorphous). Those values were used instead of the areas under the output peaks.

The raw data can then be plotted along with the final results of the Rietveld analysis (raw data, calculated, cellulose Iβ, background, amorphous and difference between raw data and calculated). The reported crystallite size or, more accurately, the domain size is based on the integral breadth (IB) of the peak:

$$\beta_i = \frac{\lambda}{L_{vol}\cos\theta} \qquad \text{Eq 2}$$

where β_i are integral breadths as proposed by (Stokes and Wilson, 1944) addressing domain-size broadening independent of crystallite shape, λ is the radiation wavelength (1.542 Å), and θ is the Bragg diffraction angle – corresponding to the (2 0 0) plane in the present case. Conceptually, Equation 2 is identical to the Scherrer (1918) equation with the constant K set to 1:

$$D = \frac{K\lambda}{\beta\cos\theta} \qquad \text{Eq 3}$$

where D is the "apparent crystallite size," and β the full width in radians 2θ of the diffraction peak measured at half maximum height (FWHM) of the instrument corrected line profile. The crystallite size can then be calculated using Equation 3. Various Rietveld software will have different equations for calculating crystallite size. See Fig. 1 for some examples of the different FWHM valus on the diffraction patterns..

Results and Discussion

Phase 2 Rietveld Modelling Tests

The Rietveld modelling procedure was tested in Phase 2 of the ILC by sending PXRD data recorded at FPInnovations for each of the three samples (noted above) to participants. The results of these tests are shown in Fig. 2. There was a relatively large number of differences in the Rietveld modelling for this step which included the CIF used (some participants disagreed with the choice of CIF provided), the approach for modelling the amorphous component, corrections implemented and fitting range. This (at least in part) leads to the lab-to-lab variability that is observed for percent crystallinity shown in Fig. 2. As a result of this test of the Rietveld procedure, several changes were implemented in the protocol. These included more detail on the recommended software packages, specification of the CIF for cellulose 1β to use for modelling (available from the Crystallography Open Database, and based on neutron data in (Nishiyama et al. 2002), two options for modelling the amorphous component, restriction of the fitting range, and two possible methods to deal with background and orientation corrections.

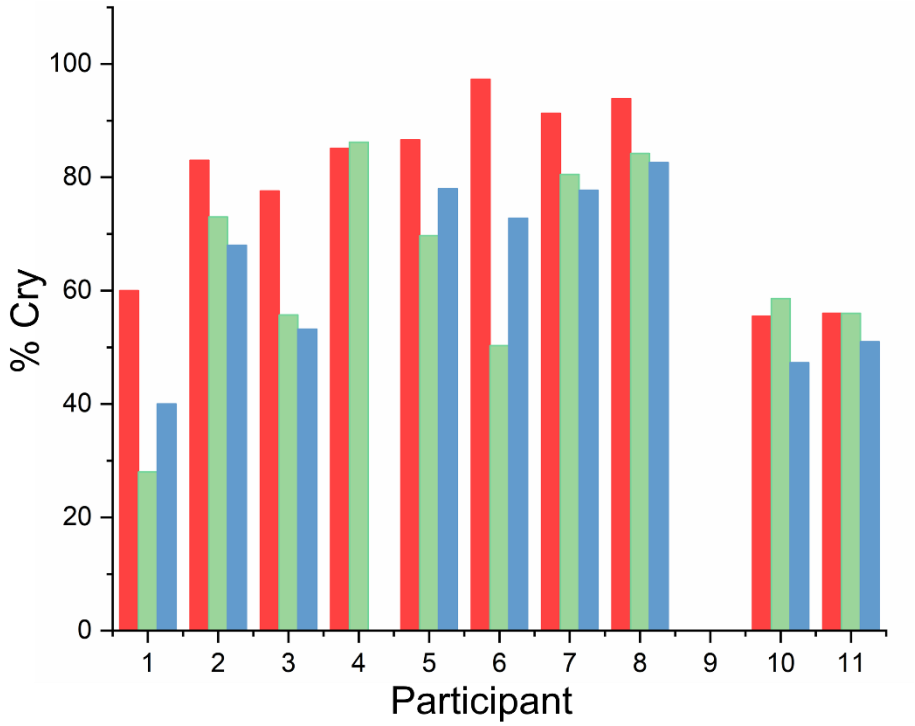


Fig. 2. % Crystallinity measured in Phase 2 Rietveld modelling tests. Data for CNC (red), CNF (green) and iCNF (blue) are shown for each participant; participant 9 did not return results. The mean % crystallinity and standard deviation for each sample are as follows: CNC (78 ± 15)%; CNF (62 ± 20)%; iCNF (61 ± 15)%.

Phase 3 Diffraction data collection

Ten participating laboratories collected PXRD in Phase 3. Diffractometers from three commercial suppliers were used; all but one lab used a Cu X-ray source with a Ni filter (one lab used a Co source) and all but one lab used a 1D detector (one lab used a NaI scintillation detector). Both zero background cells and standard sample holders were used and most participants (6 of 10) rotated the sample and recorded an instrument blank, although in some cases this was only used for optimization, rather than subtracted from the raw data. A variety of different options were used for the final instrument configuration (primarily the slits), which reflected the different diffractometers used. Data were collected from 5º to 90º 2θ in most cases, although a smaller range was used for three labs and all labs used the recommended ≤0.04° step size. Overall, the experimental conditions used for data collection followed the protocol reasonably well and represented the most common instrument configurations used for PXRD measurements. The diffractometers used by each participant as well as the instrument and experimental parameters are summarized in Table S1 of the Supporting Information. Two labs tested both dry powder and pellet samples, although only the powder samples are reported here for consistency across laboratories.

The diffraction patterns for the ten participating laboratories were very similar except for some variation at low angles due to background signals and, for lab 8, an additional signal due to the Al

sample holder. The results are illustrated in Fig. 3 which shows diffraction data before and after background correction for one CNC replicate for each laboratory. Each laboratory is assigned a code (L#); note that the lab codes are different for Phase 2 and Phase 3. The results indicate good reproducibility of the PXRD data across laboratories.

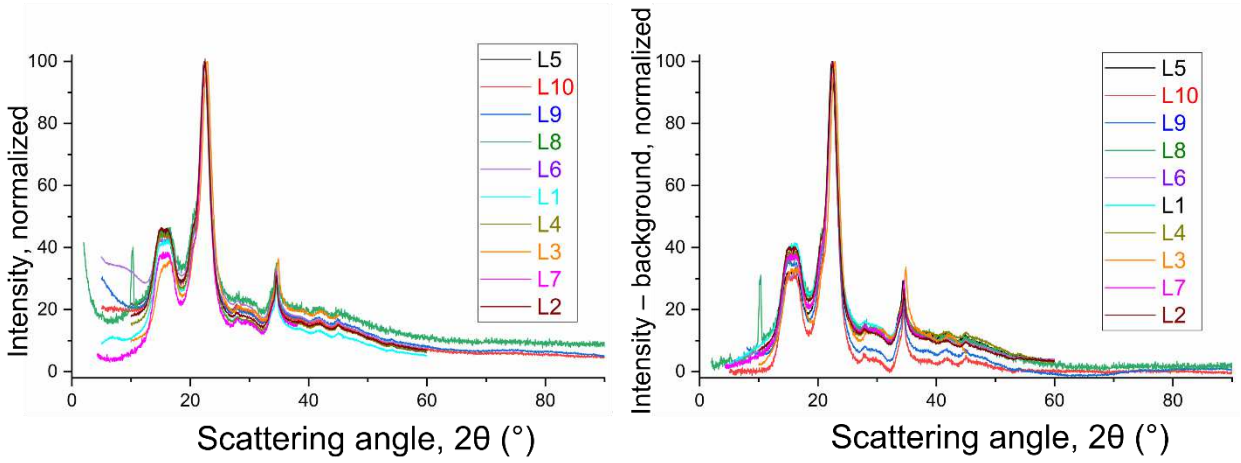
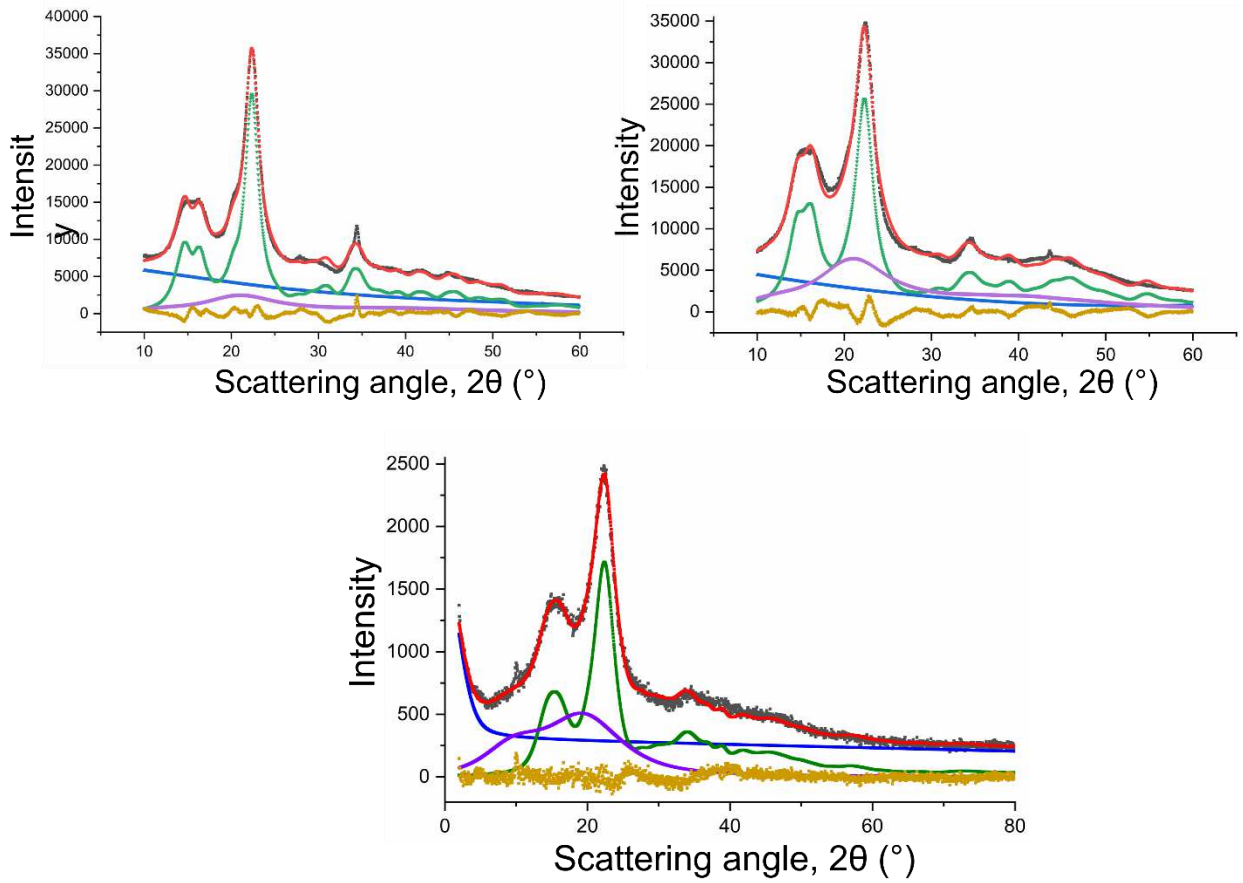


Fig. 3. Comparison of diffraction patterns for one CNC replicate for each laboratory before (left) and after (right) background correction. The data for each laboratory has been normalized based on the main peak at ~22° 2-theta. The data for L8 has an additional signal at 10° that is due to the Al sample holder used; data for L7 was collected using a Co X-ray source but converted to Cu for display purposes.

Rietveld Modelling Results

Rietveld modelling of the diffraction data used three commercial software packages (provided by the diffractometer manufacturers), MAUD, a freely available software package, and two in-house designed software packages (see Table S2). Examples of final results for three labs for a single CNC replicate are shown in Fig. 4 and Table S2 summarizes the modelling approach followed for each participating laboratory. The modelling results for one replicate for each laboratory are provided in Fig. S1, S2 and S3 for CNC, CNF and iCNF, respectively. One laboratory that used in-house software also compared results to a commercial software package and these data were used for consistency and ease of comparison to other laboratories. Both laboratories that used in-house software obtained considerably lower % Cry values than were obtained using one of the other software packages. The mean % crystallinity values obtained by each laboratory for the three samples are shown in Table 1.



407

408 **Fig. 4** Representative Rietveld modelling for one sample replicate for CNC (a), CNF (b) and iCNF
409 (c). The experimental data are shown in black and the final calculated modelling results in red,
410 with the difference between the two in gold. The crystalline cellulose, amorphous and background
411 components are displayed in green, purple and blue, respectively.

412

413 **Table 1.** Mean crystallinity percentages and associated standard deviation for each laboratory for
414 each sample.

	CNC			CNF			iCNF	
Lab	Crystallinity %	standard deviation		Crystallinity %	standard deviation		Crystallinity %	standard deviation
L1	77.6	0.9		72.4	3.1		67.02	5.1
L2	80.9	2.2		56.2	0.5		67.5	5.1
L3	71.1	1.1		55.1	1.6		59	0.8
L4	86.1	2.2		70	4.2		69.7	2.7
L5	75.8	5.7		78.5	6.7		74.3	3.5
L6[1]	72.4			60.2			60.7	
L7[2]	57.9			34	1.7		36.6	7.7
L8[3]	75.3	1.8		66.3	3.3		63.1	1.5

L9[1]	44			53			49	
L10	83	6.2		63.1	5		59.4	8.4

[1] one replicate only
[2] one fit only
[3] two samples in Al holder and one pellet

The approach to Rietveld modelling varied across laboratories, with differences in the way the amorphous phase was modelled, the availability of a background correction, the type of orientation correction used and other factors, including whether an anisotropic correction was implemented. Details on each of these factors are provided in Table S2. The final consensus results for the percent crystallinity and crystallite size for each of the 3 samples are shown in Figs. 5 and 6 and were calculated using the NIST consensus builder with the Bayes-Laplace model (NIST Consensus Builder) which provides the uncertainty weighted median as a consensus value. This is an appropriate approach when potential outliers will skew the mean value. Figs. 5 and 6 show the individual laboratory results as the mean plus standard deviation (black symbols and vertical lines), as well as the final ILC consensus values (green horizontal line) and the standard uncertainty (yellow shaded area). There is considerable variation between laboratories for each of the three samples as shown by the consensus values and expanded uncertainty (based on a 95% confidence interval) for measurements of % crystallinity and crystallite size, as summarized in Table 2. Note, however, that the changes made after consideration of the Phase 2 modelling tests have had some impact in reducing the lab-to-lab variability. It should also be noted that, in addition to the uncertainty listed in Table 1, there is a relatively large dark uncertainty component that is required for estimation of the final consensus value. This is shown in the plots (vertical green lines for each data point) and accounts for a number of unknown effects that contribute to the variation between laboratories. Fig. 6 indicates that there are several data points that might be considered outliers. However experimental results should only be excluded if there is a valid experimental issue with the procedure used; the variation in modelling approaches used meant that it was not possible to exclude points based on the experimental procedure followed.

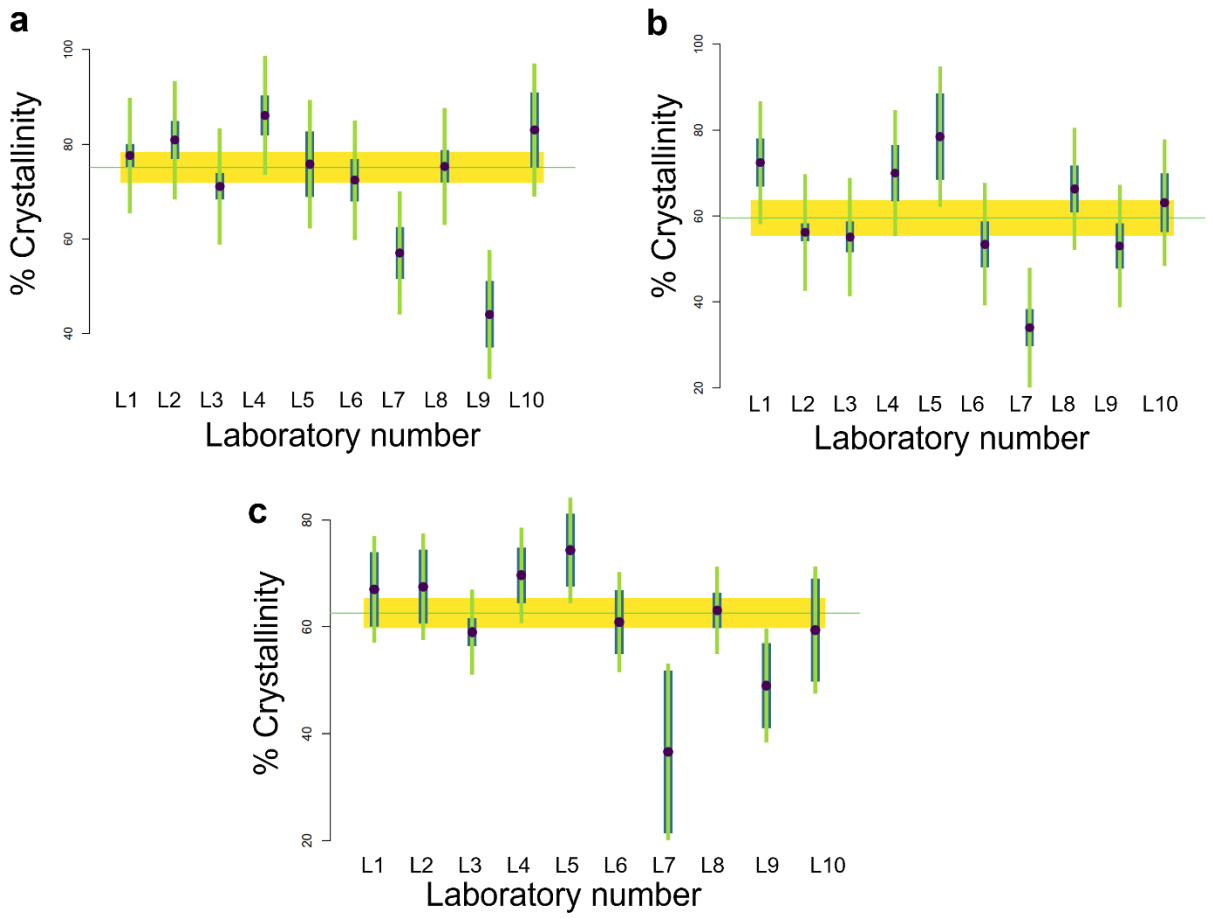


Fig. 4. NIST consensus builder plots for % Crystallinity for CNC (a), CNF (b) and iCNF (c). The mean values for all replicates for each laboratory are shown with black symbols along with the lab standard deviation (black lines). The green horizontal line is the ILC consensus value, with the yellow shaded area representing the standard uncertainty. The dark uncertainty is shown with green vertical lines.

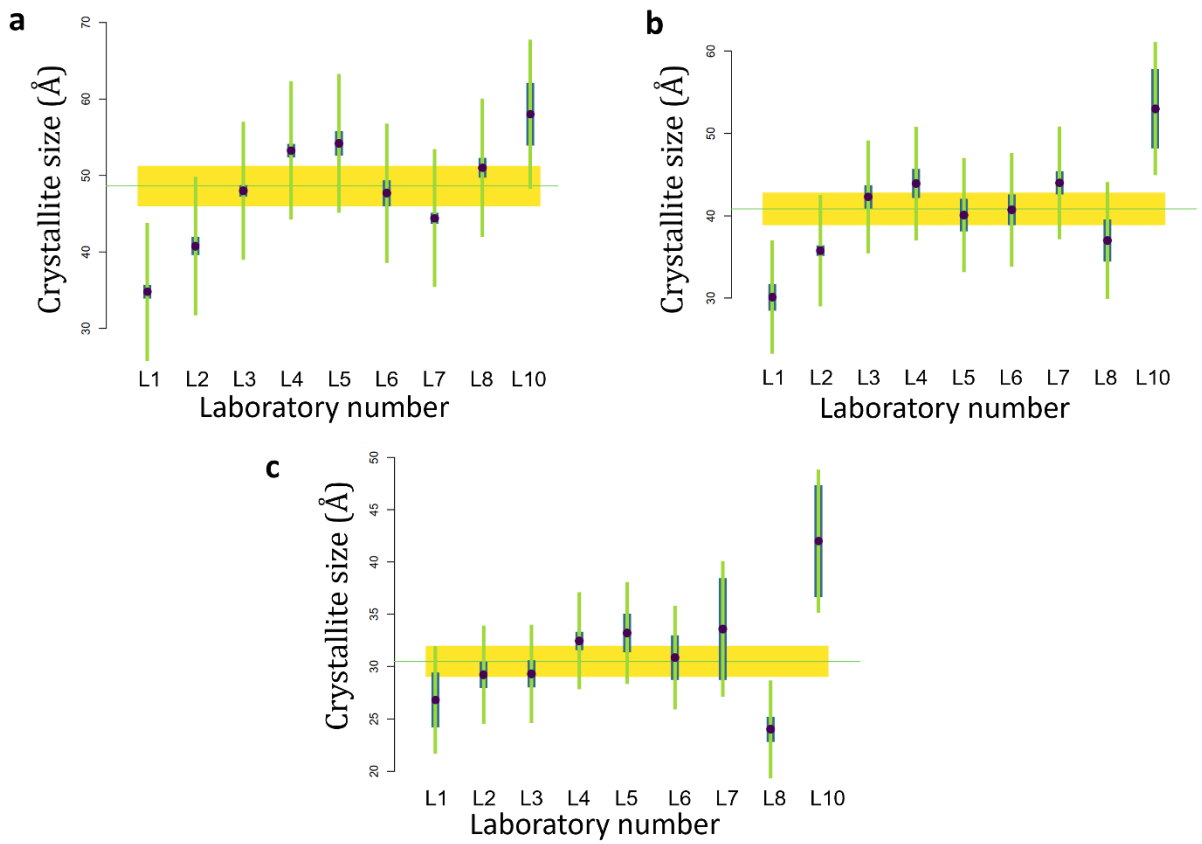


Fig. 5. NIST consensus builder plots for crystallite size (Å) for CNC (a), CNF (b) and iCNF (c). The mean values for all replicates for each laboratory are shown with black symbols along with the lab standard deviation (black lines). The green horizontal line is the ILC consensus value, with the yellow shaded area representing the standard uncertainty. The dark uncertainty is shown with green vertical lines.

Table 2. Summary of final consensus values and expanded uncertainty (based on the 95% confidence interval) for the three CNM samples. Data were estimated with the NIST consensus builder using the Bayes-Laplace model.

Sample	Crystallinity (%)		Crystallite size (Å)	
	Consensus value	Expanded uncertainty	Consensus value	Expanded uncertainty
CNC	75.1	6.4	48.6	5.1
CNF	59.6	7.9	40.8	3.9
iCNF	62.6	5.4	30.5	2.8

Despite the differences between laboratories, the individual standard deviations for each laboratory (see Figs. 5 and 6) are smaller than the expanded uncertainty for the overall ILC. This indicates that it is possible to achieve a lower standard deviation within a specific lab when the same modelling procedure is used, and to more readily make comparisons between the samples prepared using different methods. Nevertheless, one of the most important findings of this study is a clear demonstration of the level of agreement that may be expected between laboratories. This is particularly important given the relatively large number of literature reports that attempt to draw conclusions based on small (several %) differences in measured crystallinity. It should also be noted that despite the fact that Rietveld modelling can be expected to yield results with significant (10%) variation in reproducibility across laboratories, the method is based on consideration of the total signals associated with crystalline and amorphous components and represents a significant improvement over the method of Segal *et al.* (1959) which considers only intensity measurements at two specific 2θ values to determine crystallinity. Because the amorphous contribution is measured at a point where the intensity depends greatly on crystallite size (French and Santiago Cintrón 2013), the Segal *et al.* method does not accurately represent the physics of the problem and is hence intellectually unsatisfying. The widely used peak area, or peak deconvolution, method is also not satisfying in that it typically uses three to five peaks to represent crystalline material when there are numerous peaks[3] that contribute to the total observed pattern, plus an amorphous contribution.

It is worthwhile pointing out that, with 10 participating laboratories, it was challenging to identify trends as to the relative importance of the various parameters used in Rietveld modelling. For instance, although the mean percent crystallinity for labs that used cellulose II as the amorphous model was higher (by 6%) than the mean for the labs that employed a user-input function, this difference is less than the standard deviations for the two means. It is also of interest to examine the variation in the amorphous component obtained after Rietveld modelling. A comparison of the results for seven of the ten laboratories is shown in Fig. 7 and clearly illustrates the differences in size and shape for this component. Since some options are implemented differently in the various software packages, the use of a single software and more explicit instructions may improve reproducibility across laboratories. Initial tests of this hypothesis are provided in the next section.

[3] In the range of 10° to 40° 2θ (CuKα radiation) some 37 peaks make visible intensity on a calculated pattern based on the Iβ crystal structure. See Fig. 1.

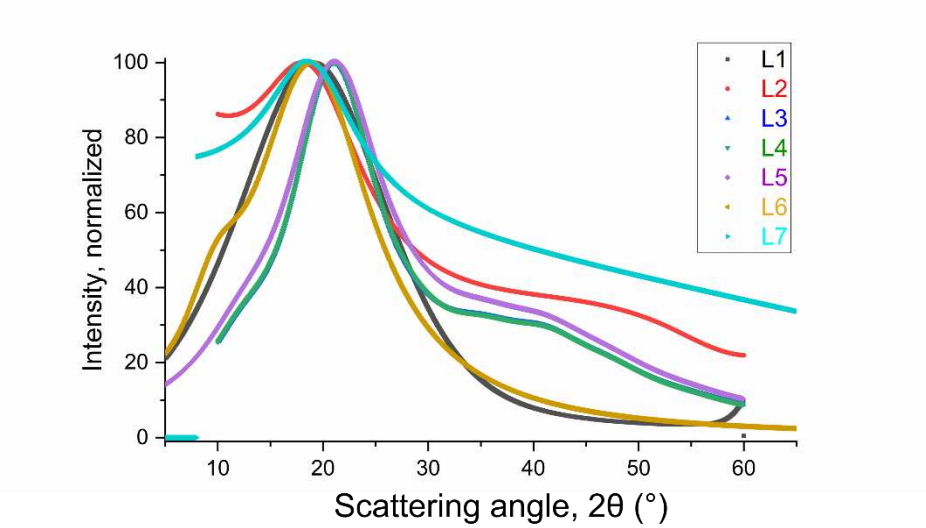


Fig. 7. Comparison of the estimated amorphous component for various participating laboratories.

Re-analysis of CNC data

The origin of the variability between laboratories was examined by re-analysing one CNC data set for each laboratory by a single analyst. The first CNC replicate was selected for each laboratory, independent of any assessment of the final fitted results. The data were used as received with subtraction of a blank scan (where available) before modelling. A constant fitting range (10-50 °) was used except for cases where the raw data did not cover the entire range. The crystalline component was modelled using the Cellulose Iβ CIF (Nishiyama et al. 2002) provided with the ILC protocol and all lattice parameters were allowed to vary. The amorphous component was modelled using the Cellulose II CIF with fixed crystal size (12 Å) and crystal lattice parameters (Langan et al. 2001). All data sets were fitted with MAUD with a polynomial background (linear or quadratic). Initial tests compared results for isotropic and anisotropic crystal sizes; the differences were small and therefore an isotropic crystal size was used for all data sets. Initial tests also indicated that the fit did not improve beyond 10 or 11 free variables so the number of variables was kept constant in subsequent fittings. Results for random and preferred orientations were compared using the March-Dollase 001 correction for the latter. This comparison was done for both linear and quadratic polynomial backgrounds. For each combination, the % crystallinity was obtained both from the MAUD fits and by summing the areas under the curves for each component. The Rwp parameter was monitored as the number of free parameters varied to assess the fit.

The MAUD results for % crystallinity are shown in Table 3. The variation in the number of parameters to fit the background suggests that at least a second degree polynomial is needed to correctly fit the data in most cases. This was more critical if the low-angle data included significant background contributions or if data was not acquired below 10 degrees. Overall the results indicate that correcting for preferred orientation did not significantly change the % crystallinity for the

CNC sample. Interestingly, the final values for the average % crystallinity have a standard deviation that is more than a factor of two smaller than observed for the original data sets but similar to the expanded uncertainty determined from the NIST consensus builder method for estimating the ILC consensus value. Note that the re-analysis of a single data set/laboratory is incompatible with the NIST consensus builder which requires multiple replicates, but one can hypothesize that reanalysis of all data for a specific sample will lead to a reduced expanded uncertainty.

Table 3. % Crystallinity calculated using an isotropic crystal size and either a linear or quadratic polynomial background for one CNC replicate for each laboratory; results obtained with both random texture and preferred orientation are provided and the % crystallinity is based on the ratio of summed areas for the crystalline and amorphous components. The data are compared to the 3-replicate mean and standard deviation obtained for each laboratory in the ILC.

Lab	Random texture		March Dollase preferred orientation correction		ILC lab mean ± standard deviation
	Linear background	Quadratic background	Linear background	Quadratic background	
1	76.9	*68.6*[a]	79.6	72.0	77.6 ± 0.9
2	95.3	77.3	96.0	80.0	80.9 ± 2.2
3	70.0	*71.5*[a]	73.6	74.5	71.1 ± 1.1
4	96.7	81.3	97.3	83.3	86.1 ± 2.2
5	89.1	77.6	86.9	78.2	76.9 ± 1.8
6	93.5	78.4	94.4	81.0	72.4[b]
7	79.5	*75.8*[a]	82.3	79.0	57.9[b]
8	80.0	67.2	82.4	72.7	75.3 ± 1.8
9	100.0	80.9	100.0	83.3	44[b]
10	93.0	79.0	94.0	81.6	83 ± 6.2
Average	87.4	75.8	86.2	78.1	72.5
Std dev	10.1	5.0	5.0	4.5	12.7

[a] A linear background was adequate for these laboratories, based on goodness of fit and visual assessment.
[b] One replicate

The average values of the lattice parameters obtained are shown in Table 4. There were some small shifts in the lattice parameters compared to the cellulose Iβ values. Effects of random vs preferred orientation and the method for modelling the background had small effects on the lattice parameters. In some cases, the ILC laboratories had allowed a relatively large variation in the lattice parameters during fitting, indicating that guidance on the level of variability that should be allowed is necessary. Based on Table 4, a variation of ± 0.2 Å from the initial CIF values could be recommended for the a, b, and c parameters and ± 0.7 ° for gamma. Finally, it is worth noting that the variability in the estimated crystallite size is also reduced when a consistent modelling approach is employed. The crystallite size for CNC based on re-analysis of one data set/laboratory was 54.9 Å (standard deviation of 1.3 Å) compared to 48.6 Å (expanded uncertainty of 5.1 Å) for ILC consensus value (Table A.1).

Table 4 Average lattice parameters and isotropic crystal size for the crystalline component. Values are the averages obtained by a single user fitting one CNC data set /laboratory. The standard deviation is shown in parentheses.

	Random texture		March-Dollase correction	
Parameter	Linear background	Quadratic background	Linear background	Quadratic background
a (Å)	7.936 (0.044)	7.929 (0.042)	7.941 (0.048)	7.925 (0.043)
b (Å)	8.103 (0.050)	8.127 (0.058)	8.104 (0.074)	8.109 (0.079)
c (Å)	10.438 (0.04)	10.442 (0.03)	10.459 (0.04)	10.435 (0.03)
$\boldsymbol{\gamma}$ (°)	95.922 (0.21)	95.89 (0.19)	95.95 (0.26)	95.87 (0.18)
Crystal size (Å)	53.22 (1.7)	55.14 (1.3)	52.69 (2.2)	54.93 (1.3)

The re-analysis results indicate that the variability between laboratories can be reduced when a single analyst and a consistent modelling approach that constrains the allowable variation of lattice parameters and the method for modelling background are employed. The data should not be interpreted to indicate that the parameters used here are necessarily optimal since there remains a lack of consensus on some of the modelling details. Nevertheless, the results do suggest that comparison of samples in a single laboratory with a consistent modelling approach will produce more reproducible results than indicated by the overall ILC consensus result and uncertainty obtained from the data collected and analyzed in 10 laboratories.

Conclusions

A significant undertaking to establish a systematic approach based on powder X-ray diffraction to measure crystallinity and potentially control the quality of cellulose nanomaterial production has been made whereby 10 international laboratories have tested a pre-defined protocol using three samples. Differences between laboratories notwithstanding, the individual standard deviations for each laboratory (see Fig. 5 and 6) were smaller than the expanded uncertainty for the overall ILC. This indicates that it is possible to achieve a lower standard deviation within a specific lab when the same modelling procedure is used, and to more readily make comparisons between the samples prepared using different methods. Nevertheless, one of the most important findings of this study is a clear demonstration of the level of agreement that may be expected between laboratories. This is particularly important given the relatively large number of literature reports that attempt to draw conclusions based on small (several %) differences in measured crystallinity. It should also be noted that despite the fact that Rietveld modelling could be expected to yield results with significant (10%) variation in reproducibility across laboratories, the method is based on consideration of the total signals associated with crystalline and amorphous components and is therefore a qualitatively major improvement over the method of Segal et al. (1959) which arbitrarily considers only intensity measurements at two specific 2θ values to determine crystallinity.

Future work that provides crystal structure data for materials from other cellulose sources would be useful as effects of orientation may be different. Reaching a consensus on the best method for modelling the diffraction peak shapes, the crystal size anisotropy, the preferred orientation and the amorphous component is anticipated to lead to results with better agreement between labs and software packages. Since some options are implemented differently in the various software packages, the use of a single software and more explicit instructions will also aid in improving the reproducibility across various laboratories and the ability to reliably distinguish between samples. Finally, it should be noted that with 10 participating laboratories and a range of potential sources of variability, it was not possible to identify meaningful trends as to the relative importance of the various parameters used in Rietveld modelling. As an example, although the mean percent crystallinity for labs that used cellulose II as the amorphous model was higher (by 6%) than the mean for the labs that employed a user-input function, this difference is less than the standard deviations for the two means.

Author contributions The original protocols were developed by WYH and further optimized by all ILC participants. The VAMAS ILC was coordinated by LJJ and WYH. Experimental work and modelling were completed by the ILC participants. Analysis of the results was coordinated by LJJ and WYH with input from participants and statistical advice from JM. The initial draft manuscript was written by WYH, LJJ, AF and NP. The final draft paper was read and edited by all authors.

Funding WYH and LJJ acknowledges financial support from Natural Resources Canada, NRCan, in part under the Transformative Technologies Program and funding from the British Columbia Ministry of Forest, Lands, Natural Resource Operations and Rural Development (BC-FLNRORD). Data for ADF and JHJ were collected at the Shared Instrument Facility at Louisiana State University by Dr. Yang Mu.

Data availability Data can be requested from LJJ at Linda.Johnston@nrc-cnrc.gc.ca.

Declarations

Conflict of interest The authors declare no competing interests.

Ethical approval Not applicable.

References

Cheary RW, Coelho AA, Cline JP (2004) Fundamental parameters line profile fitting in laboratory diffractometers. J Res Natl Inst Stand Technol 109:1-25 http://dx.doi.org/10.6028/jres.109.002

Daicho K, Tsuguyuki Saito T, Fujisawa S, Isogai A (2018) The crystallinity of nanocellulose: dispersion-induced disordering of the grain boundary in biologically structured cellulose. ACS Appl. Nano Mater. 1L5774-5785. https://doi.org/10.1021/acsanm.8b01438

Dollase WA (1986) Correction of intensities for preferred orientation in powder diffractometry: application of the March model, J Appl Cryst 19, 267-272.
https://doi.org/10.1107/S0021889886089458

Fang L, Catchmark JM (2014) Structure characterization of native cellulose during dehydration and rehydration Cellulose 21(6):3951–3963 DOI:10.1007/s10570-014-0435-8

Foster EJ, Moon RJ, Agarwal, UP, MJ, Bras J, Camarero-Espinosa S, Chan SK, Clift MJD, Cranston ED, Eichhorn SJ, Fox DM, Hamad WY, Heux L, Jean B, Korey M, Nieh W, Ong KJ, Reid MS, Renneckar S, Roberts R, Shatkin JA, Simonsen J, Stinson-Bagby K, Wanasekaraq N, Youngblood J (2018) Current characterization methods for cellulose nanomaterials. Chem Soc Rev 47:2609-2679. DOI: 10.1039/c6cs00895j

French AD (2020) Increment in evolution of cellulose crystallinity analysis. Cellulose 27:5445–5448 https://doi.org/10.1007/s10570-020-03172-z

French AD, Santiago Cintrón M (2013) Cellulose polymorphy, crystallite size, and the Segal Crystallinity Index. Cellulose 20:583–588 https://doi.org/10.1007/s10570-012-9833-y

French AD, Kim HJ (2018) Cotton Fiber Structure. Chapter 2 in Cotton Fiber: Physics, Chemistry and Biology, Ed. Fang DD https://doi.org/10.1007/978-3-030-00871-0

The Global Market for Nanocellulose (Cellulose Nanofibers, Cellulose Nanocrystals, Bacterial Nanocellulose) 2024-2034, (2024) Future Markets Inc.
https://www.researchandmarkets.com/r/ok7y67

Hamad WY, Hu TQ (2010), Structure-process-yield interrelations in nanocrystalline cellulose extraction, *Can J Chem. Eng* **88**: 392-402.
https://doi.org/10.1002/cjce.20298

Hermans PH, Weidinger A (1948) Quantitative X-Ray Investigations on the Crystallinity of Cellulose Fibers. A Background Analysis J Appl Phys 1:491-506
https://doi.org/10.1063/1.1698162

Jakubek ZJ,Chen M, Couillard M, Leng T, Liu L, Zou S, Baxa U, Clogston JD, Hamad WY, Johnston, L J (2018) Characterization challenges for a cellulose nanocrystal reference material: dispersion and particle size distributions. J Nanopart Res 20:98. https://doi. org/10.1007/s11051-018-4194-6

ISO TS 23361 Nanotechnologies - Crystallinity of cellulose nanomaterials by powder X-ray diffraction (Rietveld analysis), 2024.

Langan P, Nishiyama Y, Chanzy H (2001) X-ray structure of mercerized cellulose II at 1 Å resolution. Biomacromolecules. **2**, 410–416 https://doi.org/10.1021/bm005612q

C. F. Macrae, I. Sovago, S. J. Cottrell, P. T. A. Galek, P. McCabe, E. Pidcock, M. Platings, G. P. Shields, J. S. Stevens, M. Towler and P. A. Wood (2020 Mercury 4.0: from visualization to analysis, design and prediction, J Appl Cryst, 53:226-235 DOI: 10.1107/S1600576719014092

Mayer J, Khairy K, Howard J (2010) Drawing an elephant with four complex parameters. Am J Phys 78:648-649 DOI: 10.1119/1.3254017

Mendenhall MH, Mullen K, Cline JP (2015) An implementation of the fundamental parameters approach for analysis of X-ray powder diffraction line profiles, J. Res. Natl. Inst. Std. Tech. 120, 223-251 http://dx.doi.org/10.6028/jres.120.014

Nishiyama Y, Kuga S, Wada M, and Okano T (1997) Cellulose Microcrystal Film of High Uniaxial Orientation. Macromolecules 30*:*6395-6397 DOI: 10.1021/ma970503y

Nishiyama Y, Langan P, Chanzy H (2002) Crystal structure hydrogen-bonding system in cellulose Iβ from X-ray and neutron fiber diffraction. J Am Chem Soc 124(31):9074–9082. https://doi:10.1021/ja0257319

NIST (National Institutes of Standards and Technology) Consensus Builder. (NICOB), available at https://consensus.nist.gov/app/nicob.

Park S, Baker JO, Himmel ME et al Cellulose crystallinity index: measurement techniques and their impact on interpreting cellulase performance. Biotechnol Biofuels 3, 10 (2010). https://doi.org/10.1186/1754-6834-3-10

Popa NC, Balzar D (2008) Size-broadening anisotropy in whole powder pattern fitting. Application to zinc oxide and interpretation of the apparent crystallites in terms of physical models. J Appl Cryst 41:615–627 https://doi.org/10.1107/S0021889808012223Rietveld HM (1969) A profile refinement method for nuclear and magnetic structures. J Appl Crystallogr 2:65–71. https://doi.org/10.1107/S0021889869006558

Salem KS, Kasera NK, Rahman MA, Jameel H, Habibi Y, Eichhorn SJ, French AD, Pal L, Lucia LA (2023) Comparison and assessment of methods for cellulose crystallinity determination. Chem Soc Rev https://doi.org/10.1039/D2CS00569G

Scherrer P (1918) estimmung der Größe und der inneren Struktur von Kolloidteilchen mittels Röntgenstrahlen. Nachrichten von der Gesellschaft der Wissenschaften zu Göttingen, Mathematisch-Physikalische Klasse 1918: 98-100 http://eudml.org/doc/59018

Segal L, Creely JJ, Martin AE, Conrad CM (1959) An empirical method for estimating the degree of crystallinity of native cellulose using the X-ray diffractometer. Text Res J 29(10):786–794 https://doi:10.1177/004051755902901003

Stokes AR, Wilson AJC (1944) The diffraction of X-rays by distorted crystal aggregates—1, Proc. Phys. Soc. (London) 56, 174-181

669 Thygesen A, Oddershede J, Lilholt H, Thomsen AB, Ståhl A (2005) On the determination of
670 crystallinity and cellulose content in plant fibres. Cellulose 12:563–576
671 https://doi.org/10.1007/s10570-005-9001-8

672 Yang H, Kubicki JD (2020) A density functional theory study on the shape of the primary cellulose
673 microfibril in plants: effects of C6 exocyclic group conformation and H-bonding. Cellulose
674 27:2389–2402. https://doi.org/10.1007/s10570-020-02970-9

675 Yang H, Wang T, Oehme D, Petridis L, Hong M, Kubicki JD (2018) Structural factors affecting
676 13C NMR chemical shifts of cellulose: a computational study. Cellulose 25, 23–36.
677 https://doi.org/10.1007/s10570-017-1549-6

Supplementary Files

This is a list of supplementary files associated with this preprint. Click to download.

- ILCpaperSIFINAL.docx